

Ground-state Bethe root densities and quantum phase transitions

Jon Links and Ian Marquette

Centre for Mathematical Physics, School of Mathematics and Physics,
The University of Queensland, Brisbane, QLD 4072, Australia

E-mail: jrl@maths.uq.edu.au, i.marquette@uq.edu.au

Abstract. Exactly solvable models provide a unique method, via qualitative changes in the distribution of the ground-state roots of the Bethe Ansatz equations, to identify quantum phase transitions. Here we expand on this approach, in a quantitative manner, for two models of Bose–Einstein condensates. The first model deals with the interconversion of bosonic atoms and molecules. The second is the two-site Bose–Hubbard model, widely used to describe tunneling phenomena in Bose–Einstein condensates. For these systems we calculate the ground-state root density. This facilitates the determination of analytic forms for the ground-state energy, and associated correlation functions through the Hellmann–Feynman theorem. These calculations provide a clear identification of the quantum phase transition in each model. For the first model we obtain an expression for the molecular fraction expectation value. For the two-site Bose–Hubbard model we find that there is a simple characterisation of condensate fragmentation.

1. Introduction

In [1] Rubeni et al. studied quantum phase transitions in two bosonic models related to Bose–Einstein condensation, from the perspective of their Bethe Ansatz solutions. One model deals with the interconversion of bosonic atoms and molecules [2–4]. The other is the two-site Bose–Hubbard model, widely used to describe tunneling phenomena in Bose–Einstein condensates [5–10] and which continues to be the subject of extensive study, e.g. [11–18]. For these systems the quantum phase transition points are analogs of fixed-point bifurcations in a corresponding classical system. Crossing through a bifurcation leads to an abrupt change in the dynamical behaviour. Experimental observation of this property has been reported for a system modelled by the two-site Bose–Hubbard Hamiltonian [13], raising the potential to probe quantum systems at the macroscopic level. This feature has also been reported in a photonic context [19].

By numerically solving the Bethe ansatz equations for the ground state, it was found in [1] that there is a sharp change in the character of the root distribution in the complex plane around a particular coupling value. Through complementary computations of entanglement, fidelity, and the energy gap, it was identified that the change in the root distribution coincides with a quantum phase transition. Similar correspondences have also been witnessed in other models admitting exact Bethe ansatz solutions [20–26], which have in common that their solutions are of the *Richardson–Gaudin* form. In some literature this form is also referred to as Bethe Ansatz equations in the quasi-classical limit. See [27] and references therein for a summary of this latter point.

The goal of the present research is to provide an enhanced quantitative study of the two models considered in [1]. We will approach this from both an analytic and a numerical viewpoint. The techniques implemented are quite general and can be applied to other models with Bethe Ansatz equations of the Richardson–Gaudin form, which are the following class of coupled nonlinear algebraic equations

$$f(v_j) = \sum_{k \neq j}^M \frac{2}{v_k - v_j}, \quad (1)$$

where $f(v)$ is a rational function which can be expressed as

$$f(v) = \sum_{i=0}^k c_i v^i + \sum_{m=0}^s \frac{1}{(v - a_m)^{b_m}}.$$

Constructing the polynomial

$$Q(z) = \prod_{k=1}^M (z - v_k),$$

it satisfies

$$\frac{Q''(v_j)}{Q'(v_j)} = - \sum_{k \neq j}^M \frac{2}{v_k - v_j}.$$

Then Eq. (1) can be expressed in the polynomial form

$$\left(\prod_{m=0}^s (v_j - a_m)^{b_m} \right) Q''(v_j) + \left(\prod_{m=0}^s (v_j - a_m)^{b_m} \right) \left(\sum_{i=0}^k c_i v_j^i + \sum_{m=0}^s \frac{1}{(v_j - a_m)^{b_m}} \right) Q'(v_j) = 0.$$

Using $Q(v_j) = 0$ we can write

$$A_2(z)Q''(z) + A_1(z)Q'(z) = A_0(z)Q(z), \quad (2)$$

where $A_2(z)$, $A_1(z)$ and $A_0(z)$ are polynomials of order

$$\begin{aligned} K_2 &= \sum_{m=0}^s b_m, \\ K_1 &= k + \sum_{m=0}^s b_m, \\ K_0 &= k - 1 + \sum_{m=0}^s b_m \end{aligned}$$

respectively. Specifically,

$$\begin{aligned} A_2(z) &= \prod_{m=0}^s (z - a_m)^{b_m}, \\ A_1(z) &= \left(\sum_{i=0}^k c_i z^i + \sum_{m=0}^s \frac{1}{(z - a_m)^{b_m}} \right) \prod_{n=0}^s (z - a_n)^{b_n}. \end{aligned}$$

The polynomials $Q(z)$ and $A_0(z)$ can be constructed by inserting expansions

$$Q(z) = \sum_{k=0}^M \alpha_k z^k, \quad A_0(z) = \sum_{j=0}^{K_0} \beta_j z^j \quad (3)$$

into (2), yielding a system of linear equations. We take $\alpha_M = 1$ with the remaining α_k and β_j to be determined numerically. The roots of the polynomial $Q(z)$ can be extracted once the α_k have been computed. We will follow the numerical procedure given in [23]. Related approaches are described in [24, 26, 28–31].

For the two models to be analysed below it is found that the roots associated with the ground state lie on the real line. In such an instance the discrete root density is computed from the numerical solution via

$$\tilde{\rho}(v_j) = \frac{1}{(M-1)(v_{j+1} - v_j)}, \quad j = 1, \dots, M-1$$

such that

$$\sum_{j=1}^{M-1} \tilde{\rho}(v_j)(v_{j+1} - v_j) = 1. \quad (4)$$

On the other hand, in the limit $M \rightarrow \infty$ a root density $\rho(v)$ with support on an interval $[\mathfrak{a}, \mathfrak{b}] \subseteq \mathbb{R}$ can be introduced as a solution of the continuum limit of (1), viz. the singular integral equation

$$\lim_{M \rightarrow \infty} \frac{f(v)}{M} = P \int_{\mathfrak{a}}^{\mathfrak{b}} \frac{2\rho(w)}{w-v} dw, \quad (5)$$

where P denotes the Cauchy principal value of the integral, subject to

$$\int_{\mathfrak{a}}^{\mathfrak{b}} \rho(w) dw = 1 \quad (6)$$

such that (6) is the continuum analogue of (4).

In this paper we will compute both the discrete and continuum root densities for two models studied in [1], which will be explicitly provided below. Moreover, it will be demonstrated how the root densities can be used to perform calculations which identify a quantum phase transition in each system.

2. Atomic-molecular Bose-Einstein condensate model

The first Hamiltonian to be studied takes the following form

$$H = \mu \hat{N}_c + \Omega(\hat{a}^\dagger \hat{b}^\dagger \hat{c} + \hat{c}^\dagger \hat{a} \hat{b}), \quad (7)$$

where the operators $\{\hat{j}, \hat{j}^\dagger | \hat{j} = \hat{a}, \hat{b}, \hat{c}\}$ are canonical bosonic creation and annihilation operators, and $\hat{N}_j = \hat{j}^\dagger \hat{j}$. The parameter μ governs the external potential and Ω is the amplitude for interconversion of atoms, associated with labels a and b , and molecules, associated with the label c . The Hamiltonian (7) is a particular limit of a more general model for hetero-nuclear atomic-molecular Bose-Einstein condensates, introduced in [2–4]. The form (7) appeared many years ago in quantum optics [32], and it is also the analogue of the homo-nuclear model studied by Vardi, Yurovsky, and Anglin [33].

This system is integrable and exactly solvable. The Hamiltonian (7) commutes with the total number of particles $\hat{N} = \hat{N}_a + \hat{N}_b + 2\hat{N}_c$ and the atomic imbalance $\hat{J} = \hat{N}_a - \hat{N}_b$. We denote the eigenvalues of \hat{N} and \hat{J} by N and J respectively. The energy eigenvalues are given by [2]

$$E = -\Omega \sum_{j=1}^M v_j, \quad (8)$$

where the v_j are roots of the associated Bethe Ansatz equations

$$\frac{J+1}{v_j} - v_j - \frac{\mu}{\Omega} = \sum_{k \neq j}^M \frac{2}{v_k - v_j} \quad (9)$$

with $M = (N - J)/2$ and $J = 0, 1, \dots, N$. We also introduce the fractional imbalance $k = J/N \in [-1, 1]$.

2.1. Continuum limit approximation

The Bethe Ansatz equations (9) in the continuum limit $M \rightarrow \infty$ take the form of a singular integral equation. For technical reasons it is most convenient to consider the integral form (5) as an approximation for the Bethe Ansatz equations (9) for large, but finite, M . This yields

$$P \int_{\mathfrak{a}}^{\mathfrak{b}} \frac{2\rho(w)}{w-v} dw = \frac{1}{M} \left(\frac{J+1}{v} - v - \frac{\mu}{\Omega} \right) \quad (10)$$

such that M appears explicitly as a variable. This approximation will allow us to determine the scaling properties of certain quantities as $M \rightarrow \infty$, which is necessary for an intermediate step in the calculations below.

Next we adopt the following Ansatz for the root density

$$\rho(v) = \sqrt{(\mathfrak{b}-v)(v-\mathfrak{a})} \left(A + \frac{B}{v} \right) \quad (11)$$

with A and B some constants yet to be determined. Due to the branch cut in (11) the integral in the left-hand side of (10) can be evaluated over a contour in the complex plane which encloses the interval $[\mathfrak{a}, \mathfrak{b}]$. The contour integral can be evaluated by computing the residues at the origin and at the point at infinity. See Appendix B of [23] for further details. Performing these calculations produces

$$\begin{aligned} \int_{\mathfrak{a}}^{\mathfrak{b}} \rho(v) dv &= \frac{A\pi}{8}(\mathfrak{a}-\mathfrak{b})^2 + \frac{B\pi}{2}(\sqrt{\mathfrak{a}}-\sqrt{\mathfrak{b}})^2, \\ P \int_{\mathfrak{a}}^{\mathfrak{b}} \frac{2\rho(w)}{w-v} dw &= A\pi(\mathfrak{a}+\mathfrak{b}-2v) + 2B\pi \left(\frac{\sqrt{\mathfrak{a}\mathfrak{b}}}{v} - 1 \right). \end{aligned}$$

This leads to the following four equations for the parameters A , B , \mathfrak{a} and \mathfrak{b} in terms of μ , Ω and M :

$$\begin{aligned} 1 &= \frac{A\pi}{8}(\mathfrak{a}-\mathfrak{b})^2 + \frac{B\pi}{2}(\sqrt{\mathfrak{a}}-\sqrt{\mathfrak{b}})^2, \\ J+1 &= 2\pi BM\sqrt{\mathfrak{a}\mathfrak{b}}, \\ 1 &= 2\pi AM, \\ -\frac{\mu}{\Omega} &= \pi A(\mathfrak{a}+\mathfrak{b})M - 2\pi BM. \end{aligned} \quad (12)$$

Rearranging the second and third equations to obtain

$$A = \frac{1}{2\pi M}, \quad B = \frac{J+1}{2\pi M\sqrt{\mathfrak{a}\mathfrak{b}}},$$

and inserting in the two other equations, yields

$$\begin{aligned} M &= \frac{1}{16}(\mathfrak{a}-\mathfrak{b})^2 + \frac{J+1}{4\sqrt{\mathfrak{a}\mathfrak{b}}}(\sqrt{\mathfrak{a}}-\sqrt{\mathfrak{b}})^2, \\ -\frac{\mu}{\Omega} &= \frac{\mathfrak{a}+\mathfrak{b}}{2} - \frac{J+1}{\sqrt{\mathfrak{a}\mathfrak{b}}}. \end{aligned}$$

Setting

$$\alpha = -\frac{\mu}{\Omega\sqrt{2N}},$$

we can manipulate the above to obtain the following quartic equation for $\sqrt{\mathbf{a}\mathbf{b}}$:

$$(\mathbf{a}\mathbf{b})^2 + 2(1 - \alpha^2)N\mathbf{a}\mathbf{b} - 4(J + 1)\alpha\sqrt{2N}\sqrt{\mathbf{a}\mathbf{b}} - 3(J + 1)^2 = 0. \quad (13)$$

Assuming $J = O(N^0)$ we have the following asymptotics:

$$\mathbf{a}\mathbf{b} \sim \begin{cases} 2(\alpha^2 - 1)N, & \alpha > 1, \\ 2^{5/3}(J + 1)^{2/3}N^{1/3}, & \alpha = 1, \\ \left(\frac{J + 1}{f}\right)^2 N^{-1}, & \alpha < 1, \end{cases} \quad (14)$$

where

$$f = \frac{2(1 - \alpha^2)}{2\sqrt{2}\alpha + \sqrt{2\alpha^2 + 6}}.$$

Conversely, for $J = O(N)$ such that $k = J/N \neq 0$, we have $\mathbf{a}\mathbf{b} = O(N)$ for all α .

In [2] the coupling $\alpha = 1$ was identified as a quantum phase transition point when $k = 0$, but it was also found that there is no transition for $k \neq 0$. Here, the quantum phase transition manifests as a change in the scaling of $\mathbf{a}\mathbf{b}$ when $k = 0$, while there is no such change for $k \neq 0$. For $k = 0$ there is a distinct qualitative change in the ground-state root density upon crossing $\alpha = 1$. This is illustrated in Fig. 1, where both the discrete root density and continuum approximation are plotted for $M = 50$, $J = 0$ and particular values of $\alpha > 1$. As the coupling parameter α decreases the quantity \mathbf{a} , the minimum endpoint of the support for the root density, moves towards zero. For comparison, analogous densities are plotted in Fig. 2 for $M = 50$, $J = 0$ and particular values of $\alpha < 1$. The main qualitative difference between the two figures is the behaviour of the root density at \mathbf{a} . In Fig. 1, the continuum limit approximation vanishes at $\mathbf{a} > 0$. In Fig. 2, the continuum limit approximation diverges at $\mathbf{a} = 0$. Also note the change in the vertical scale of the second panel in Fig. 2.

2.2. Ground-state energy and molecular fraction expectation value

Having established that a sudden change occurs in the ground-state root density upon crossing the point $\alpha = 1$, we next demonstrate how this manifests in certain physical quantities. First we consider the ground-state energy. From (8,11), the continuum limit approximation becomes

$$\begin{aligned} E &= -\Omega \int_{\mathbf{a}}^{\mathbf{b}} \rho(v)v dv \\ &= \mu \left(\frac{N + 1}{2} + \frac{(J + 1)^2}{2\mathbf{a}\mathbf{b}} \right) - \frac{(J + 1)\mu}{2\alpha\sqrt{2N}\sqrt{\mathbf{a}\mathbf{b}}} \left(\mathbf{a}\mathbf{b} - \frac{(J + 1)^2}{\mathbf{a}\mathbf{b}} \right), \end{aligned} \quad (15)$$

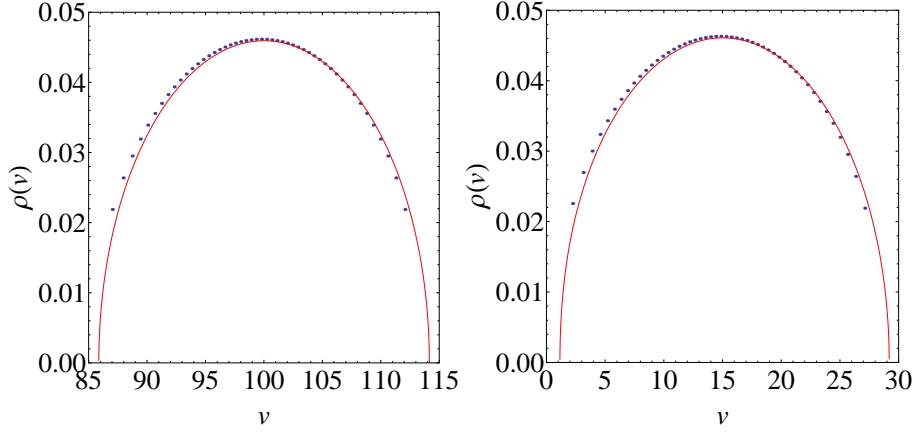


Figure 1: Atomic-molecular Bose–Einstein condensate model: Ground-state roots densities for $M = 50$, $J = 0$ and $\Omega = 1$. The discrete root density is depicted by points and the solid line is the continuum limit approximation for (a) $\mu = -100$ ($\alpha \approx 7.07$), (b) $\mu = -15$ ($\alpha \approx 1.06$). In both cases the continuum limit approximation vanishes at $\mathbf{a} > 0$.

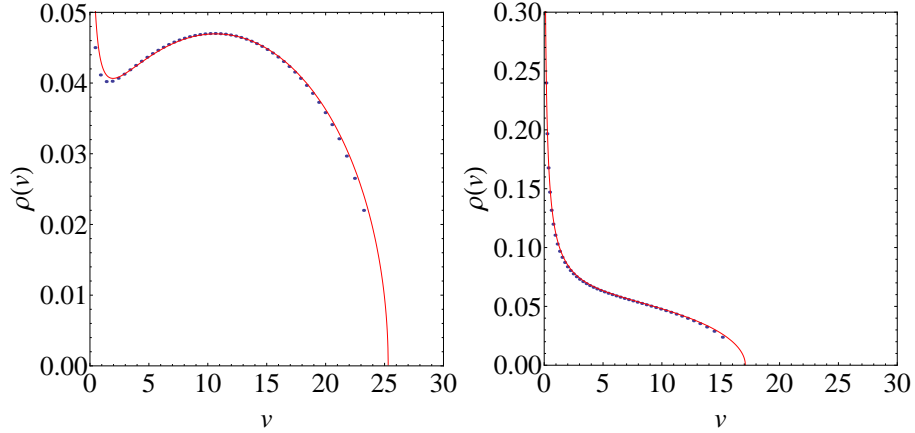


Figure 2: Atomic-molecular Bose–Einstein condensate model: Ground-state roots densities for $M = 50$, $J = 0$ and $\Omega = 1$. The discrete root density is depicted by points and the solid line is the continuum limit approximation for (a) $\mu = -11$ ($\alpha \approx 0.78$), (b) $\mu = -1$ ($\alpha \approx 0.07$). In both cases the continuum limit approximation diverges at $\mathbf{a} = 0$.

where the expression above has been obtained via contour integral techniques and simplified using the Eqs. (12). Use of (14) then yields the leading order behaviour

$$E \sim \begin{cases} \frac{\mu N}{2}, & \alpha \geq 1, \\ \frac{\mu N}{2} \left(1 + f^2 + \frac{1}{\sqrt{2}\alpha} f^3 \right), & \alpha \leq 1. \end{cases} \quad (16)$$

μ	E_{cl}	E_{num}	ΔE	% error
-100	-5000.000	-5000.500	0.500	0.001
-15	-750.000	-754.718	4.718	0.625
-11	-566.498	-570.397	3.899	0.684
-1	-289.531	-290.763	1.232	0.423

Table 1: Atomic-molecular Bose–Einstein condensate model: Ground-state energy for $N = 100$, $J = 0$ and $\Omega = 1$. For each value of μ , E_{cl} denotes the value obtained from the continuum limit approximation (16), while E_{num} is obtained from (8) and the numerical solution of the Bethe Ansatz equations (9). The final columns show the difference and the relative percentage error respectively. The quantum phase transition point is $\mu_c \approx -14.14$.

It is somewhat surprising that the above result is independent of J , despite (14,15) being J -dependent.

Table 1 compares the ground-state energy from the continuum approximation against results obtained by numerically solving the Bethe Ansatz equations (9) and using (8). The agreement is excellent. It is anticipated that the continuum limit approximation becomes exact as $N \rightarrow \infty$. However taking this limit from the outset is problematic. In particular this can be seen through the N -dependence of (14), which is required to compute (16) via (15).

To conclude this discussion, we show how this approach enables the characterisation of the quantum phase transition at $\alpha = 1$ via an order parameter. Recall that the Hellmann-Feynmann theorem can be stated as

$$\left\langle \frac{\partial H}{\partial \lambda} \right\rangle = \frac{\partial E}{\partial \lambda},$$

where in general H is a Hamiltonian depending on a coupling parameter λ , and the expectation value is with respect to an eigenstate of energy E . Defining

$$\mathcal{O} = \frac{2 \langle N_c \rangle}{N},$$

which is the molecular fraction expectation value, it follows for the Hamiltonian (7) that

$$\mathcal{O} = \frac{2}{N} \frac{\partial E}{\partial \mu}.$$

From (16) we obtain for the ground-state molecular fraction expectation value

$$\mathcal{O} \sim \begin{cases} 1, & \alpha \geq 1, \\ 1 + f^2 + \left(2\alpha f + \frac{3}{\sqrt{2}} f^2 \right) f', & \alpha \leq 1, \end{cases} \quad (17)$$

where f' denotes the derivative of f with respect to α . This calculation shows that the quantum phase transition point $\alpha = 1$ separates a pure molecular phase and a mixed atomic-molecular phase.

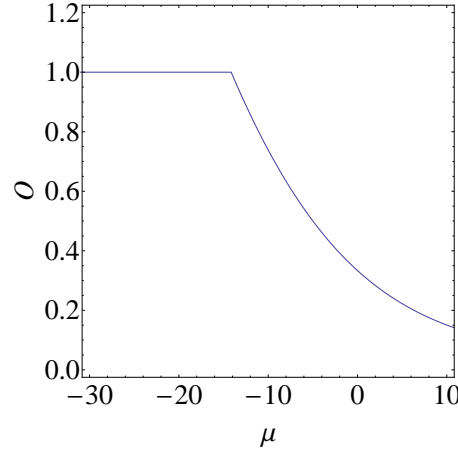


Figure 3: Atomic-molecular Bose–Einstein condensate model: Molecular fraction expectation value O , as given by the continuum approximation result (17), as a function of the coupling parameter μ for $N = 100$, $J = 0$ and $\Omega = 1$. The quantum phase transition point is $\mu_c \approx -14.14$. Compare with Fig. 7 of [2] which has similar qualitative features.

3. Symmetric two-site Bose–Hubbard model

The Hamiltonian of the symmetric two-site Bose–Hubbard model is given by [5–12, 14–18]

$$H = \frac{k}{8}(\hat{N}_1 - \hat{N}_2)^2 - \frac{\mathcal{E}}{2}(\hat{a}_1^\dagger \hat{a}_2 + \hat{a}_2^\dagger \hat{a}_1), \quad (18)$$

where for $i, j = 1, 2$

$$[\hat{a}_i, \hat{a}_j^\dagger] = \delta_{ij}, \quad [\hat{a}_i, \hat{a}_j] = [\hat{a}_i^\dagger, \hat{a}_j^\dagger] = 0,$$

and $\hat{N}_j = \hat{a}_j^\dagger \hat{a}_j$. Setting $\hat{N} = \hat{N}_1 + \hat{N}_2$, it can be verified that $[H, \hat{N}] = 0$. We denote the eigenvalues of \hat{N} by N . Note that because (18) is invariant under the interchange of labels 1 and 2, the subspaces of symmetric and antisymmetric states are invariant under the action of (18).

Previous studies [6, 8, 10] have identified a quantum phase transition in the attractive regime $k < 0$. Setting

$$\lambda = -\frac{kN}{2\mathcal{E}}, \quad (19)$$

the transition takes place at $\lambda = 1$. This phenomenon was examined in [1] with attention to the nature of the ground-state roots of the following Bethe Ansatz equations

$$\frac{\mathcal{E}v_j^2 + k(1 - N)v_j - \mathcal{E}}{kv_j^2} = \sum_{k \neq j}^N \frac{2}{v_k - v_j}. \quad (20)$$

We prefer to use an alternative form, which first appeared in [34]. For simplicity we

restrict to the case where N is even. The alternative Bethe Ansatz equations read

$$\frac{2\mathcal{E}}{k} + \frac{2\mu}{v_j - 1} + \frac{2\mu}{v_j + 1} = \sum_{k \neq j}^M \frac{2}{v_k - v_j}, \quad (21)$$

such that the associated energy is given by

$$E = \frac{kN^2}{8} + \mathcal{E} \sum_{j=1}^M v_j, \quad (22)$$

the total particle number is

$$N = 2M + 4\mu - 1,$$

and $\mu = 1/4$ for symmetric states and $\mu = 3/4$ for antisymmetric states. It can be checked that the ground state lies in the symmetric subspace of the full space of states, e.g. see [6], in which case $N = 2M$.

The equivalence of the two forms of Bethe Ansatz equations (20) and (21) was established in [35]‡. The advantage of using the form (21) is that the ground-state roots are real-valued and lie in the interval $[-1, 1]$, which was deduced by numerical solution of the Bethe Ansatz equations (21) using the techniques in [23].

3.1. Continuum limit approximation

Adopting the procedure of the previous example we consider the integral form (5) as an approximation of (21) for large, but finite, M :

$$\frac{4\alpha}{M} + \frac{1}{M(v-1)} + \frac{1}{M(v+1)} = P \int_{\mathfrak{a}}^{\mathfrak{b}} \frac{4\rho(w)}{w-v} dw, \quad (23)$$

where $-1 \leq \mathfrak{a} < \mathfrak{b} \leq 1$ and we have set $\rho = 1/4$. Taking the density to have the form

$$\rho(v) = \sqrt{(\mathfrak{b}-v)(v-\mathfrak{a})} \left(\frac{A}{v-1} + \frac{B}{v+1} \right) \quad (24)$$

it follows from (23) that

$$\begin{aligned} & \frac{4\alpha}{M} + \frac{1}{M(v-1)} + \frac{1}{M(v+1)} \\ &= -4\pi A \left(\frac{\sqrt{(1-\mathfrak{a})(1-\mathfrak{b})}}{v-1} + 1 \right) + 4\pi B \left(\frac{\sqrt{(1+\mathfrak{a})(1+\mathfrak{b})}}{v-1} - 1 \right), \end{aligned}$$

while the normalisation condition (6) gives

$$\frac{\pi A}{2}(\mathfrak{a} + \mathfrak{b} - 2 + 2\sqrt{(1-\mathfrak{a})(1-\mathfrak{b})}) + \frac{\pi B}{2}(\mathfrak{a} + \mathfrak{b} + 2 - 2\sqrt{(1+\mathfrak{a})(1+\mathfrak{b})}) = 1.$$

‡ There is a typographical error in the energy expression (18) of Ref. [35]

Setting

$$\begin{aligned}\mathfrak{c} &= \sqrt{(1 - \mathfrak{a})(1 - \mathfrak{b})}, \\ \mathfrak{d} &= \sqrt{(1 + \mathfrak{a})(1 + \mathfrak{b})}\end{aligned}$$

it is deduced that

$$\begin{aligned}A &= -\frac{1}{8\pi N \mathfrak{c}}, \\ B &= \frac{1}{8\pi N \mathfrak{d}}, \\ A + B &= \frac{1}{\pi \lambda}.\end{aligned}$$

Eliminating A and B then leads to the equations

$$\begin{aligned}\lambda(\mathfrak{d}^{-1} - \mathfrak{c}^{-1}) &= 8N, \\ 2N(\mathfrak{d}^2 - \mathfrak{c}^2) + \lambda(\mathfrak{d}^{-1} + \mathfrak{c}^{-1}) &= 4\lambda(2N + 1).\end{aligned}$$

The leading order solution valid for $\lambda > 1$ is

$$\begin{aligned}\mathfrak{c} &\sim \frac{1}{4(1 - \lambda^{-1})N}, \\ \mathfrak{d} &\sim \frac{1}{4(1 + \lambda^{-1})N},\end{aligned}$$

which shows that $\mathfrak{a} \sim -1$ and $\mathfrak{b} \sim 1$. For $\lambda < 1$

$$\begin{aligned}\mathfrak{c} &\sim 2\sqrt{1 - \lambda}, \\ \mathfrak{d} &\sim \frac{\lambda}{8N},\end{aligned}$$

yielding

$$\begin{aligned}\mathfrak{a} &\sim -1, \\ \mathfrak{b} &\sim 2\lambda - 1.\end{aligned}$$

In Fig. 4, both the discrete root density and continuum approximation are plotted for $M = 50$, corresponding to $N = 100$, and particular values of $\lambda < 1$. As the coupling parameter λ increases the quantity \mathfrak{b} , the maximum endpoint of the support for the root density, moves towards 1. For comparison, analogous densities are plotted in Fig. 5 for $M = 50$ and particular values of $\lambda > 1$. The main qualitative difference between the two figures is the behaviour of the root density at \mathfrak{b} . In Fig. 4, the continuum limit approximation vanishes at $\mathfrak{b} < 1$. In Fig. 5, the continuum limit approximation diverges at $\mathfrak{b} = 1$. In both cases the root density is divergent at $\mathfrak{a} = -1$.

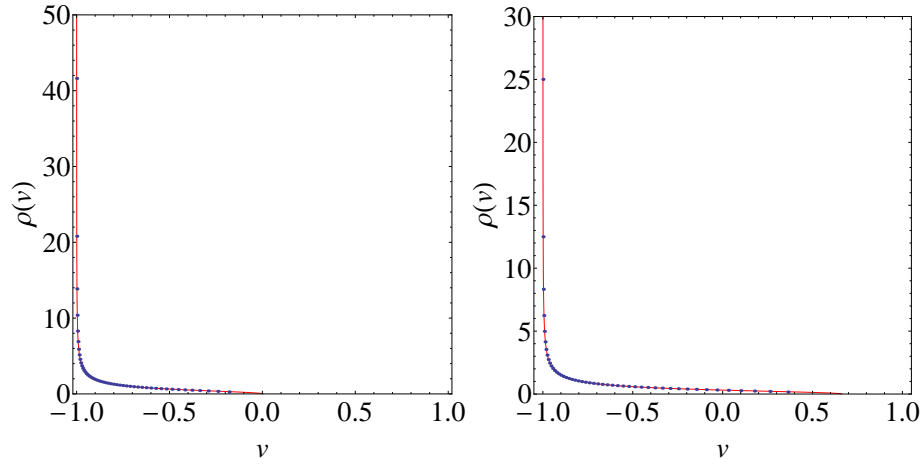


Figure 4: Symmetric two-site Bose–Hubbard model: Ground-state roots densities for $M = 50$ ($N = 100$) and $\mathcal{E} = 1$. The discrete root density is depicted by points and the solid line is the continuum limit approximation for (a) $k = -1/100$ ($\lambda = 1/2$), (b) $k = -1/60$ ($\lambda = 5/6$). Here, the continuum limit approximation vanishes at $\mathfrak{b} < 1$.

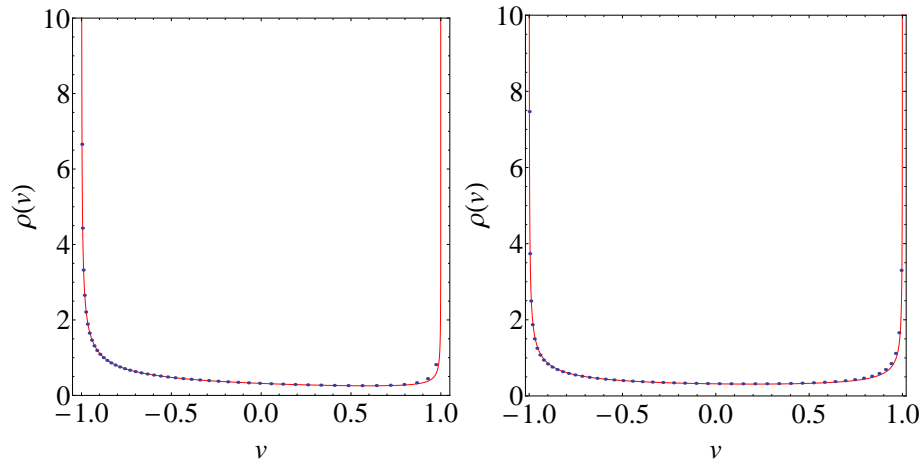


Figure 5: Symmetric two-site Bose–Hubbard model: Ground-state roots densities for $M = 50$ ($N = 100$) and $\mathcal{E} = 1$. The discrete root density is depicted by points and the solid line is the continuum limit approximation for (a) $k = -1/30$ ($\lambda = 5/3$), (b) $k = -1/10$ ($\lambda = 5$). In both cases the continuum limit approximation diverges at $\mathfrak{b} = 1$.

k	E_{cl}	E_{num}	ΔE	% error
-1/100	-50.000	-50.146	0.146	0.291
-1/60	-50.000	-50.292	0.292	0.581
-1/30	-56.667	-56.836	0.169	0.297
-1/10	-130.000	-130.051	0.051	0.039

Table 2: Symmetric two-site Bose–Hubbard model: Ground-state energy for $N = 100$ and $\mathcal{E} = 1$. For each value of k , E_{cl} denotes the value obtained from the continuum limit approximation (25), while E_{num} is obtained from (22) and the numerical solution of the Bethe Ansatz equations (21). The final columns show the difference and the relative percentage error respectively. The quantum phase transition point is $k_c = -1/50$.

3.2. Ground-state energy and correlation functions

From (22,24) the continuum limit approximation for the ground-state energy reads

$$\begin{aligned}
E &= \frac{kN^2}{8} + \frac{\mathcal{E}N}{2} \int_a^b v \rho(v) dv \\
&= \frac{kN^2}{8} \left(1 - \frac{2}{\lambda}\right) \int_a^b v \rho(v) dv \\
&= \frac{kN^2}{8} \left(1 - \frac{2}{\lambda}\right) \int_a^b dv \sqrt{(b-v)(v-a)} \left(\frac{Av}{v-1} + \frac{Bv}{v+1}\right).
\end{aligned}$$

Using the results of the previous subsection leads to the simple leading order result for the ground-state energy:

$$E \sim \begin{cases} -\frac{\mathcal{E}N}{2}, & \lambda \leq 1, \\ -\frac{\mathcal{E}N}{4} (\lambda + \lambda^{-1}), & \lambda \geq 1. \end{cases} \quad (25)$$

As before, we appeal to the Hellmann-Feynman theorem to compute ground-state correlation functions. Following [9] we define the coherence correlator to be given by

$$\begin{aligned}
\theta &= \frac{1}{N} \langle \hat{a}_1^\dagger \hat{a}_2 + \hat{a}_2^\dagger \hat{a}_1 \rangle \\
&= \frac{2}{N} \frac{\partial E}{\partial \mathcal{E}}
\end{aligned}$$

and the imbalance fluctuation as

$$\begin{aligned}
\chi &= \frac{1}{N^2} \langle (\hat{N}_1 - \hat{N}_2)^2 \rangle \\
&= \frac{4}{N^2} \frac{\partial E}{\partial k}.
\end{aligned}$$

From (25) these are found to be given by

$$\theta = \begin{cases} 1 & \lambda \leq 1 \\ \lambda^{-1} & \lambda \geq 1 \end{cases}$$

$$\chi = \begin{cases} 0 & \lambda \leq 1 \\ 1 - \lambda^{-2} & \lambda \geq 1 \end{cases}$$

The above formulae complement the asymptotic results of [9], which were derived for the repulsive case $k > 0$.

Finally, we can also use the above results to associate the quantum phase transition point $\lambda = 1$ [12,18,36] with the onset of condensate fragmentation. Following [12,18,36], denoting the ground state by $|\psi\rangle$ consider the one-body density matrix

$$\rho^{(1)} = \frac{1}{N} \begin{pmatrix} \langle \psi | \hat{a}_1^\dagger \hat{a}_1 | \psi \rangle & \langle \psi | \hat{a}_1^\dagger \hat{a}_2 | \psi \rangle \\ \langle \psi | \hat{a}_2^\dagger \hat{a}_1 | \psi \rangle & \langle \psi | \hat{a}_2^\dagger \hat{a}_2 | \psi \rangle \end{pmatrix}.$$

The system is said to be unfragmented if the eigenvalues of $\rho^{(1)}$ are 0 and 1, otherwise the system is said to be fragmented. Exploiting the symmetry of the Hamiltonian (18) upon interchange of the labels 1 and 2, it is found that for $\lambda \leq 1$

$$\rho^{(1)} = \frac{1}{2} \begin{pmatrix} 1 & 1 \\ 1 & 1 \end{pmatrix}$$

with eigenvalues 0 and 1, while for $\lambda \geq 1$

$$\rho^{(1)} = \frac{1}{2} \begin{pmatrix} 1 & \lambda^{-1} \\ \lambda^{-1} & 1 \end{pmatrix}$$

with eigenvalues $\frac{1}{2} \pm \frac{1}{2\lambda}$. Thus, the phase transition point $\lambda = 1$ separates fragmented and unfragmented phases.

4. Conclusion

In this work we have re-examined the studies conducted in [1] for an atomic-molecular Bose–Einstein condensate model and the symmetric two-site Bose–Hubbard model. By calculation of the ground-state Bethe root density in the limit of infinite number of roots, we obtain analytic expressions for the ground-state energy which shows excellent agreement with numerical calculations. This in turn allows for the calculation of correlation functions through use of the Hellmann-Feynman theorem. These techniques are not specific to the two models considered here, but have wider applicability to other systems such as [20–26] as mentioned in the Introduction. For new applications, we specifically identify the wide scope to apply these methods to generalisations of the two-site Bose–Hubbard model to cases which include non-linear tunneling [36–38] and multi-level systems [39].

Acknowledgments

The research of J. L. is supported by the Australian Research Council through Discovery Project DP110101414, and I. M. is supported by Discovery Early Career Researcher Award DE130101067. We thank Angela Foerster for insightful advice, and Inna Lukyanenko for her astute comments.

References

- [1] Rubeni D, Foerster A, Mattei E and Roditi I 2012 Quantum phase transition in Bose-Einstein condensate from a Bethe Ansatz perspective, *Nucl. Phys. B* **856** 698
- [2] Duncan M, Foerster A, Links J, Mattei E, Oelkers N and Tonel A 2007 Emergent quantum phases in a heteronuclear molecular Bose-Einstein condensate model, *Nucl. Phys. B* **767** 227
- [3] Zhou L, Zhang W, Jiang H Y L L and Pu H 2007 Properties of a coupled two species atom-heteronuclear molecule condensate, *Phys. Rev. A* **75** 043603
- [4] Zhou L, Qian J, Pu H, Zhang W and Ling H Y 2008 Phase separation in two-species atomic Bose-Einstein condensate with interspecies Feshbach resonance *Phys. Rev. A* **78** 053612
- [5] Milburn G J, Corney J, Wright E M and Walls D F 1997 Quantum dynamics of an atomic Bose-Einstein condensate in a double-well potential *Phys. Rev. A* **55** 4318
- [6] Cirac J I, Lewenstein M, Mølmer K and Zoller P 1998 Quantum superposition states of Bose-Einstein condensates *Phys. Rev. A* **57** 1208
- [7] Leggett A J 2001 Bose-Einstein condensation in the alkali gases: Some fundamental concepts *Rev. Mod. Phys.* **73** 307
- [8] Kohler S and Sols F 2002 Oscillatory decay of a two-component Bose-Einstein condensate *Phys. Rev. Lett.* **89** 060403
- [9] Zhou H-Q, Links J, McKenzie R H and Guan X-W 2003 Exact results for a tunnel-coupled pair of trapped Bose-Einstein condensates *J. Phys. A: Math. Gen.* **36** L113
- [10] Pan F and Draayer J P 2005 Quantum critical behavior of two coupled Bose-Einstein condensates *Phys. Lett. A* **339** 403
- [11] Pérez-Campos C, González-Alonso J R, Castaños O and López-Peña R 2010 Entanglement and localization of a two-mode Bose-Einstein condensate *Ann. Phys.* **325** 325
- [12] Julia-Diaz B, Martorell J, and Polls A 2010 Bose-Einstein condensates on slightly asymmetric double-well potentials *Phys. Rev. A* **81** 063625
- [13] Zibold T, Nicklas E, Gross C and Oberthaler M K 2010 Classical bifurcation at the transition from Rabi to Josephson dynamics *Phys. Rev. Lett.* **105** 204101
- [14] Buonsante P, Burioni R, Vescovi E and Vezzani A 2012 Quantum criticality in a bosonic Josephson junction *Phys. Rev. A* **85** 043625
- [15] Simon L and Strunz W T 2012 Analytical results for Josephson dynamics of ultracold bosons *Phys. Rev. A* **86** 053625
- [16] Jezek D M, Capuzzi P and Cataldo H M 2013 Two-mode effective interaction in a double-well condensate *Phys. Rev. A* **87** 053625
- [17] Graefe E-M, Korsch H J and Strzys M P 2014 Bose-Hubbard dimers, Viviani's windows and pendulum dynamics *J. Phys. A: Math. Theor.* **47** 085304
- [18] Sakmann K, Streltsov A I, Alon O E and Cederbaum L S 2014 Universality of fragmentation in the Schrödinger dynamics of bosonic Josephson junctions *Phys. Rev. A* **89** 023602
- [19] Abbarchi M et al. 2013 Macroscopic quantum self-trapping and Josephson oscillations of exciton polaritons *Nature Phys.* **9** 275
- [20] Dunning C, Ibañez M, Links J, Sierra G and Zhao S-Y 2010 Exact solution of the $p + ip$ pairing Hamiltonian and a hierarchy of integrable models *J. Stat. Mech.: Theor. Exp.* P08025

- [21] Rombouts S M A, Dukelsky J and Ortiz G 2010 Quantum phase diagram of the integrable $p_x + ip_y$ fermionic superfluid *Phys. Rev. B* **82** 224510
- [22] Lerma H S, Rombouts S M A, Dukelsky J and Ortiz G 2011 Integrable two-channel $p_x + ip_y$ -wave model of a superfluid *Phys. Rev. B* **84** 100503(R)
- [23] Marquette I and Links J 2012 Generalised Heine-Stieltjes and Van Vleck polynomials associated with degenerate, integrable BCS models, *J. Stat. Mech.* P08019
- [24] Lerma H S and Dukelsky J 2013 The Lipkin–Meshkov–Glick model as a particular limit of the $SU(1, 1)$ Richardson–Gaudin integrable models *Nucl. Phys. B* **870** 421
- [25] Marquette I and Links J 2013 Integrability of an extended $d + id$ -wave pairing Hamiltonian *Nucl. Phys. B* **866** 378
- [26] Van Raemdonck M, De Baerdemacker S and Van Neck D 2014 Exact solution of the $p_x + ip_y$ pairing Hamiltonian by deforming the pairing algebra *Phys. Rev. B* **89** 155136
- [27] Lukyanenko I, Isaac P S and Links J 2014 On the boundaries of quantum integrability for the spin-1/2 Richardson–Gaudin system, *Nucl. Phys. B* **886** 364
- [28] Pan F, Bao L, Zhai L, Cui X and Draayer J P 2011 The extended Heine-Stieltjes polynomials associated with a special LMG model *J. Phys. A: Math. Theor.* **44** 39
- [29] Faribault A, El Araby O, Strater C and Gritsev V 2011 Gaudin model solver based on the Bethe ansatz/ordinary differential equations correspondence *Phys. Rev. B* **83** 235124
- [30] El Araby O, Gritsev V and Faribault A 2012 Bethe ansatz and ordinary differential equation correspondence for degenerate Gaudin models *Phys. Rev. B* **85** 115130
- [31] Guan X, Launey K D, Xie M, Bao L, Pan F and Draayer J P 2012 Heine-Stieltjes correspondence and the polynomial approach to the standard pairing problem *Phys. Rev. C* **86** 024313
- [32] Walls D F and Barakat R 1970 Quantum-mechanical amplification and frequency conversion with a trilinear Hamiltonian *Phys. Rev. A* **1** 446
- [33] Vardi A, Yurovsky V A and Anglin J R 2001 Quantum effects on the dynamics of a two-mode atom-molecule Bose-Einstein condensate *Phys. Rev. A* **64** 063611
- [34] Enol'skii V Z, Kuznetsov V B and Salerno M 1993 On the quantum inverse scattering method for the DST dimer *Physica D* **68** 138
- [35] Links J and Zhao S-Y 2009 A Bethe Ansatz study of the ground state energy for the repulsive Bose–Hubbard dimer *J. Stat. Mech.: Theor. Exp.* P03013
- [36] Zhu Q, Zhang Q and Wu B 2014 Extended Bose-Hubbard model with pair tunneling: spontaneous symmetry breaking, effective ground state and fragmentation, arXiv:1404.6346
- [37] Liang J-Q, Liu J-L, Li W-D and Li Z-J 2009 Atom-pair tunneling and quantum phase transition in the strong-interaction regime *Phys. Rev. A* **79** 033617
- [38] Tonel A P and Ymai L H 2013 Integrable models for Bose-Einstein condensates in a double-well potential formulated from Holstein-Primakoff transformations *J. Phys. A: Math. Theor.* **46** 125202
- [39] Santos G, Foerster A and Roditi I 2013 A bosonic multi-state two-well model *J. Phys. A: Math. Theor.* **46** 265205